# EFFECT OF WORKING-FLUID MIXTURES ON ORGANIC RANKINE CYCLE SYSTEMS: HEAT TRANSFER AND COST ANALYSIS

Oyeniyi A. Oyewunmi and Christos N. Markides*

Clean Energy Processes (CEP) Laboratory, Department of Chemical Engineering,
Imperial College London, London SW7 2AZ, United Kingdom
*E-mail: c.markides@imperial.ac.uk
Web-page: www.imperial.ac.uk/cep

## ABSTRACT

The present paper considers the employment of working-fluid mixtures in organic Rankine cycle (ORC) systems with respect to heat transfer performance, component sizing and costs, using two sets of fluid mixtures: *n*-pentane + *n*-hexane and R-245fa + R-227ea. Due to their non-isothermal phase-change behaviour, these zeotropic working-fluid mixtures promise reduced exergy losses, and thus improved cycle efficiencies and power outputs over their respective pure-fluid components. Although the fluid-mixture cycles do indeed show a thermodynamic improvement over the pure-fluid cycles, the heat transfer and cost analyses reveal that they require larger evaporators, condensers and expanders; thus, the resulting ORC systems are also associated with higher costs, leading to possible compromises. In particular, 70 mol% *n*-pentane + 30 mol% *n*-hexane and equimolar R-245fa + R-227ea mixtures lead to the thermodynamically optimal cycles, whereas pure *n*-pentane and pure R-227ea have lower costs amounting to 14% and 5% per unit power output over the thermodynamically optimal mixtures, respectively.

## 1. INTRODUCTION

Recently, the selection of working fluids for organic Rankine cycle (ORC) systems has received close attention, including a particular interest in multi-component fluid mixtures, due to the opportunities they offer in improving thermodynamic performance. Various authors have carried out investigations to demonstrate and quantify these benefits, which have shown that working-fluid mixtures can exhibit an improved thermal match with the heat source compared to the isothermal profile of (isobaric) evaporation of pure-component fluids, therefore reducing exergy losses due to heat transfer, and increasing thermal and exergy efficiencies (Angelino and di Paliano, 1998; Garg et al., 2013; Wang et al., 2010).

Investigators have carried out both experimental and theoretical studies across a range of heat-source temperatures into the benefits of employing refrigerant (Sami, 2010; Chen et al., 2011; Aghahosseini and Dincer, 2013), hydrocarbon (Heberle et al., 2012; Shu et al., 2014), and siloxane (Dong et al., 2014), working-fluid mixtures. Compared to pure fluids, binary mixtures showed increased power outputs by up to 30% and thermal efficiencies by over 15% in some cases. Excellent second law analyses have also shown significant potential benefits (Lecompte et al., 2014). (Some exceptions to these general trends have also been reported (Li et al., 2014).) Additionally, fluid mixtures can be used to adjust the environmental and safety-related properties of ORC working fluids or to improve design parameters of system components. At the same time, some investigators have begun to develop and apply advanced computer-aided molecular design (CAMD) methodologies (Papadopoulos et al., 2010; Lampe et al., 2014) with a view towards identifying or designing optimal fluids for ORC systems.

While these efforts have demonstrated the potential advantages of working-fluid mixtures, notably in terms of power output and efficiency, many of the associated conclusions have been derived strictly based on thermodynamic cycle analyses that do not fully consider the expected heat transfer performance between the heat source/sink and working-fluid streams in the heat exchangers of ORC engines. In particular, the heat transfer and cost implications of using working-fluid mixtures have not been properly addressed. Refrigerant mixtures are known to exhibit reduced heat-transfer coefficients (HTCs) compared to their pure counterparts (Jung et al., 1989). Specifically, HTCs for refrigerants mixtures are

usually lower than the 'ideal' values, linearly interpolated between the mixture components. This, coupled with the reduced temperature difference between the heat source/sink and the working-fluid mixture, will invariably lead to larger and more expensive heat exchangers in an ORC system. Therefore, although working-fluid mixtures may allow a thermodynamic advantage over single-component working fluids, they may also lead to higher system costs owing to a deterioration in their thermal performance.

By presenting a method for evaluating the HTCs of working-fluid mixtures, this work aims to explore the effects of using such mixtures on the heat transfer processes in ORC engines, which are important in understanding the role that these fluids play on the overall system performance and cost. A simple ORC engine model is presented that incorporates a suitable heat transfer description of the heat exchangers used for the heat addition and heat rejection processes. The heat exchangers are discretized along their lengths into segments (accounting for phase-change and single-phase regions), with suitable estimates of the HTCs in the different segments. Overall HTCs and heat-transfer areas (HTAs) are then evaluated, and simple cost models are used to estimate the relative costs of the components, and by extension of the entire engine. Using a selection of alkane and refrigerant working-fluid mixtures, the heat transfer characteristics and ORC-system equipment/component costs are thus investigated.

## 2. THERMODYNAMIC OPTIMIZATION

We begin with a simple thermodynamic optimization of an ORC system in a specified geothermal application with two sets of working-fluid mixtures: the *n*-hexane + *n*-pentane alkane system; and the R-245fa + R-227ea refrigerant system. Earlier studies have shown that these mixtures can provide significant thermodynamic benefits in ORC systems (Lecompte et al., 2014; Chys et al., 2012; Braimakis et al., 2014). Further, pentane and the selected refrigerants are presently being used in actual installations, especially in geothermal ORC setups, such as the one considered here.

### 2.1 ORC Model

We consider a sub-critical, non-regenerative ORC, consisting of four basic processes (pumping, heat addition, expansion and heat rejection), carried out by an organic working fluid (wf). Briefly, for completeness, the power required to pump the working fluid from State 1 (saturated liquid) to State 2 is:

$$\dot{W}_{\text{pump}} = \dot{m}_{\text{wf}} \left(h_2 - h_1\right) = \dot{m}_{\text{wf}} \left(h_{2\text{s}} - h_1\right) / \eta_{\text{is,pump}} \,. \tag{1}$$

The heat extracted from the heat source is transferred to the working fluid assuming no heat losses and no pressure losses (*i.e.*, an isobaric process). In our engine, the working fluid exits this process as a saturated vapour (State 3), since superheating has been shown to be detrimental to ORC performance (Oyewunmi et al., 2014). Thus, the rate of heat input from the heat source (hs) is given by:

$$\dot{Q}_{\text{in}} = \dot{m}_{\text{hs}}\, c_{p,\text{hs}} \left(T_{\text{hs,in}} - T_{\text{hs,out}}\right) \text{; and, } \dot{Q}_{\text{in}} = \dot{m}_{\text{wf}} \left(h_3 - h_2\right) . \tag{2}$$

The power generated as the working fluid is expanded to State 4 is:

$$\dot{W}_{\text{exp}} = \dot{m}_{\text{wf}} \left(h_3 - h_4\right) = \eta_{\text{is,exp}}\, \dot{m}_{\text{wf}} \left(h_3 - h_{4\text{s}}\right) . \tag{3}$$

During heat rejection, the working fluid transfers heat to a cooling stream (cs) at a rate given by:

$$\dot{Q}_{\text{out}} = \dot{m}_{\text{wf}} \left(h_4 - h_1\right) \text{; and, } \dot{Q}_{\text{out}} = \dot{m}_{\text{cs}}\, c_{p,\text{cs}} \left(T_{\text{cs,out}} - T_{\text{cs,in}}\right) . \tag{4}$$

The pump and expander isentropic efficiencies ($\eta_{\text{is,pump}}$ and $\eta_{\text{is,exp}}$) are taken as 75%, while all necessary fluid properties are calculated with REFPROP 9.1 (Kunz and Wagner, 2012; Lemmon et al., 2013).

### 2.2 Application

A wide variety of fluid streams can be used as ORC-system heat sources, including thermal oil (*e.g.*, in solar applications), process streams (*e.g.*, in industrial applications), geothermal water/steam, exhaust/flue

gases, *etc*. For the purpose of this work, it is more appropriate to consider liquid-phase source and sink streams; gaseous streams would dominate the thermal resistances on the source and sink sides of the heat exchangers, thereby overshadowing the thermal resistances on the working-fluid vapour and liquid streams, and limiting the information we hope to derive by employing different working-fluid mixtures. Thus, the heat source selected in the present work is a hot-water stream from the 80 $kW_e$ Birdsville geothermal ORC power-plant in Australia (Beardsmore et al., 2015), with an inlet temperature ($T_{hs,in}$) of 98 °C and a flow rate of 27 $kg.s^{-1}$ (inlet enthalpy flow of 8.8 $MW_{th}$). This is typical of what is obtainable from other (low-pressure) geothermal reservoirs and also (low-grade) waste-heat streams in industrial processes. The heat sink is a water stream at ambient conditions (in at 20 °C; out at 30 °C).

An optimization problem is set up to maximize the expansion power-output ($\dot{W}_{exp}$) and, concurrently, the cycle thermal and exergy efficiencies ($\eta_{th}$ and $\eta_{ex}$) for the specified heat-source enthalpy flow, while specifying that all of the working-fluid cycles are subject to the same (theoretical) total heat input from the source ($\dot{Q}_{in}$ = 1 $MW_{th}$; $T_{hs,out}$ = 89.2 °C). While this latter constraint does not represent the actual working condition in the Birdsville plant, it is imposed in order to ensure the same overall heat-exchange duty across the working-fluid mixtures, thus enabling a uniform basis for comparison. The objective function definition assumes that the pumping-power requirement is at least an order of magnitude smaller than the expansion power-output, $\dot{W}_{pump} \ll \dot{W}_{exp}$. The decision variables are the evaporation and condensation pressures, while an additional constraint concerns the heat exchangers' pinch conditions (≥ 10 °C).

### 2.3 Optimal Cycles with Working-Fluid Mixtures

The ORC is optimized for maximum $\dot{W}_{exp}$, using the Interior Point algorithm (Byrd et al., 1999). The optimal power outputs and associated operating pressures are presented in Figure 1, and the expander performance parameters are presented in Figure 2. All other cycle parameters are given in Table 1.

**Table 1: ORC optimization results**

| $x_{C_6H_{14}}$ | $\eta_{th}$ | $\eta_{ex}$ | $w_{exp}$ | $\dot{W}_{pump}$ | $\dot{m}_{wf}$ | $\dot{m}_{cs}$ | $\dot{Q}_{Ph}$ | $\dot{Q}_{Ev}$ | $\dot{Q}_{Dsh}$ | $\dot{Q}_{Cn}$ | $x_{227ea}$ | $\eta_{th}$ | $\eta_{ex}$ | $w_{exp}$ | $\dot{W}_{pump}$ | $\dot{m}_{wf}$ | $\dot{m}_{cs}$ | $\dot{Q}_{Ph}$ | $\dot{Q}_{Ev}$ | $\dot{Q}_{Dsh}$ | $\dot{Q}_{Cn}$ |
|---|---|---|---|---|---|---|---|---|---|---|---|---|---|---|---|---|---|---|---|---|---|
| | % | % | kJ/kg | kW | kg/s | kg/s | kW | kW | kW | kW | | % | % | kJ/kg | kW | kg/s | kg/s | kW | kW | kW | kW |
| 0.0 | 7.79 | 39.5 | 33.5 | 1.41 | 2.37 | 21.4 | 251 | 749 | 81.0 | 841 | 0.0 | 7.65 | 39.5 | 16.7 | 2.84 | 4.74 | 21.4 | 284 | 715 | 62.0 | 861 |
| 0.1 | 8.24 | 41.6 | 36.5 | 1.33 | 2.29 | 21.3 | 260 | 740 | 84.1 | 833 | 0.1 | 8.00 | 41.5 | 17.5 | 3.48 | 4.78 | 21.3 | 318 | 682 | 68.5 | 851 |
| 0.2 | 8.53 | 43.1 | 38.5 | 1.24 | 2.25 | 21.2 | 266 | 734 | 86.9 | 828 | 0.2 | 8.12 | 42.4 | 17.3 | 4.05 | 4.92 | 21.3 | 339 | 661 | 72.4 | 846 |
| 0.3 | 8.71 | 43.9 | 39.9 | 1.15 | 2.21 | 21.2 | 270 | 730 | 89.3 | 824 | 0.3 | 8.12 | 42.7 | 16.7 | 4.64 | 5.13 | 21.3 | 356 | 644 | 75.4 | 843 |
| 0.4 | 8.70 | 43.8 | 40.1 | 1.04 | 2.20 | 21.2 | 267 | 732 | 89.9 | 823 | 0.4 | 8.07 | 42.8 | 15.9 | 5.31 | 5.40 | 21.3 | 373 | 627 | 77.8 | 841 |
| 0.5 | 8.67 | 43.6 | 40.0 | 0.94 | 2.19 | 21.2 | 266 | 733 | 90.8 | 822 | 0.5 | 8.03 | 43.0 | 15.1 | 6.12 | 5.72 | 21.3 | 393 | 607 | 80.5 | 839 |
| 0.6 | 8.64 | 43.4 | 39.8 | 0.87 | 2.19 | 21.2 | 265 | 735 | 91.9 | 822 | 0.6 | 7.87 | 42.6 | 14.0 | 6.97 | 6.11 | 21.4 | 410 | 589 | 82.5 | 839 |
| 0.7 | 8.56 | 43.0 | 39.2 | 0.79 | 2.21 | 21.2 | 263 | 737 | 92.7 | 822 | 0.7 | 7.60 | 41.7 | 12.8 | 7.83 | 6.57 | 21.4 | 426 | 575 | 84.3 | 840 |
| 0.8 | 8.43 | 42.3 | 38.1 | 0.72 | 2.23 | 21.2 | 259 | 740 | 92.7 | 822 | 0.8 | 7.32 | 40.8 | 11.6 | 8.77 | 7.09 | 21.5 | 442 | 559 | 86.0 | 842 |
| 0.9 | 8.19 | 41.1 | 36.3 | 0.64 | 2.27 | 21.3 | 252 | 748 | 91.4 | 826 | 0.9 | 7.04 | 39.9 | 10.5 | 9.79 | 7.64 | 21.6 | 460 | 540 | 86.9 | 843 |
| 1.0 | 7.85 | 39.3 | 33.8 | 0.55 | 2.34 | 21.4 | 240 | 760 | 88.5 | 833 | 1.0 | 6.74 | 38.9 | 9.51 | 10.8 | 8.23 | 21.6 | 478 | 522 | 86.4 | 846 |

Of the 1 $MW_{th}$ heat inflow to the cycle, roughly ~75% is used to evaporate the alkane working fluids (50% – 70% for the refrigerants), while the rest is used for pre-heating the fluids to their bubble points. On average, about 0.85 MW is rejected during the condensation process. A working-fluid mixture with $x_{C_6H_{14}}$ = 0.3 results in the cycle with the highest power output and efficiency. The (pure) *n*-hexane cycle has the lowest power output (Figure 1a), followed closely by the *n*-pentane cycle; their power outputs are 10.5% and 10.1% lower than that of the optimal mixture, respectively. For the R-245fa + R-227ea system, the equimolar mixture ($x_{R\text{-}227ea}$ = 0.5) is the optimal working fluid (Figure 1b).

The working-fluid mixtures with *n*-hexane fractions between 30 mol% and 60 mol% have the highest power outputs and also the lowest working-fluid flow-rates (from Table 1). This results in cycles with the highest specific work-outputs (defined as $w_{exp} = \dot{W}_{exp}/\dot{m}_{wf}$), with $x_{C_6H_{14}}$ = 0.4 having the highest. The pure fluids have the highest mass flow-rates and this, coupled with their lower work-outputs, results in cycles with the lowest work densities, which are about ~16% lower than that of the optimal fluid-mixture. For the R-245fa + R-227ea system, the optimal working-fluid flow-rate increases monotonically from pure R-245fa to pure R-227ea, and R-227ea has the cycle with the lowest specific work.

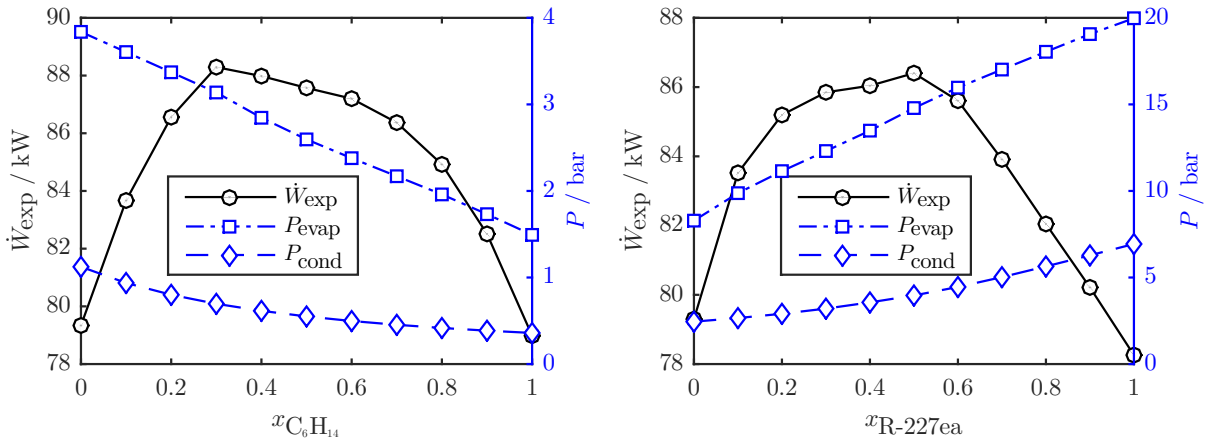


(a) *n*-pentane + *n*-hexane (b) R-245fa + R-227ea

**Figure 1: Optimal expander power-output and corresponding operating phase-change pressure**

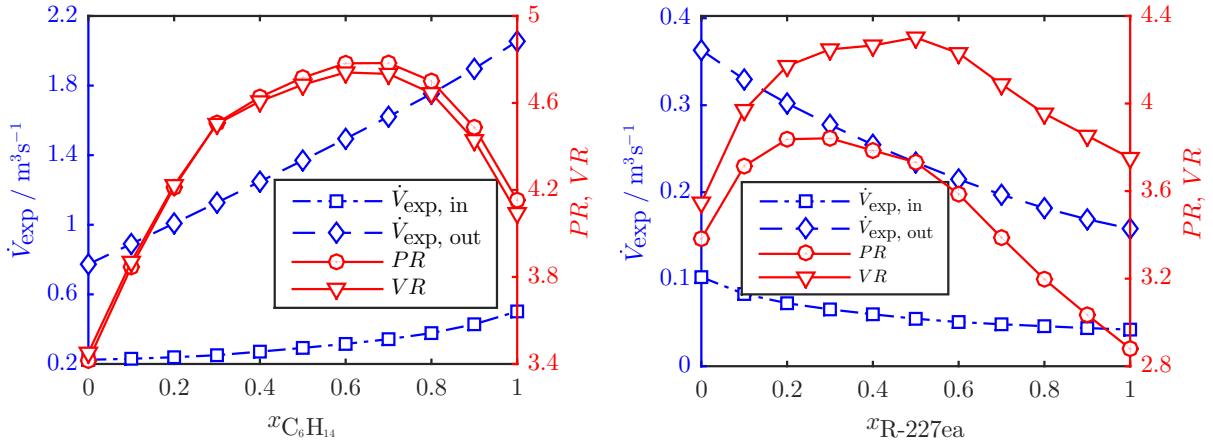


(a) *n*-pentane + *n*-hexane (b) R-245fa + R-227ea

**Figure 2: Expander volumetric flow-rate, volume and pressure ratio at optimal power output**

The temperature glides (not shown) are smaller in the evaporator than in the condenser. In both heat exchangers these follow a parabolic variation with $x$, reaching a maximum of 6 – 8 K at the equimolar mixture (*n*-pentane + *n*-hexane) and 6 – 9 K at $x_{R\text{-}227ea} = 0.3$ (R-245fa + R-227ea). These do not directly correspond to the optimal mixtures, but are close. In fact, the temperature glide is a reasonably good predictor of the maximum power-output in our study, since high power-output mixtures have relatively high temperature glides, which are also closer to the external heat source and sink temperature changes (8 and 10 K). Although this holds true for closely related binary mixtures, it has been suggested that mixtures of highly dissimilar fluids may not follow this trend (Li et al., 2014; Oyewunmi et al., 2014).

The optimal evaporation and condensation pressures (Figure 1a and 1b, RHS axes) reduce linearly from *n*-pentane (R-227ea) to *n*-hexane (R-245fa). This is because the saturation pressures of *n*-pentane (R-227ea) are higher than those of *n*-hexane (R-245fa) at the same temperature, since the critical temperature of *n*-pentane (R-227ea) is lower than that of *n*-hexane (R-245fa). In the R-245fa + R-227ea system, the entire condensation process occurs at above atmospheric pressures, whereas in the *n*-pentane + *n*-hexane system, only *n*-pentane condenses at above atmospheric conditions (the other working fluids condense at sub-atmospheric pressures). The pumping power (while being negligible compared to the expander output) mirrors the behaviour of the optimal evaporation pressure in both working-fluid systems.

The volumetric flow-rates through the expander, $\dot{V}_{exp}$ (Figure 2a and 2b, LHS axes) are linear, increasing steadily from *n*-pentane (R-227ea) to *n*-hexane (R-245fa) due to the reduction in the saturation pressures during evaporation and condensation at higher concentrations of *n*-hexane (R-245fa). The pressure ra-

tio, *PR*, and expansion ratio, *VR*, (Figure 2a and 2b, RHS axes) follow similar trends, with a minimum observed for one of the pure-fluid components (*n*-pentane and R-227ea, respectively), and a maximum observed for a fluid mixture. The low expansion-ratios and volumetric flow-rates for the pure components suggest they would require smaller expanders than the mixtures, potentially leading to cost savings. Also, they would require fewer expansion stages, further increasing the potential cost savings.

## 3. HEAT TRANSFER ANALYSIS OF OPTIMAL CYCLES

In the previous section we demonstrated the thermodynamic benefits of employing working-fluid mixtures in ORCs, especially for cases when the heat source and sink profiles are constrained. As expected, there are working-fluid mixtures that realize higher power outputs and efficiencies than both pure fluids as a result of the temperature glides during the phase change processes. The associated expansion and pressure ratios of such working-fluid mixtures are comparable to those of the pure working-fluids.

However, these results were derived purely from a thermodynamic perspective; the effects of such mixtures on the heat transfer processes in the heat exchangers, and especially the evaporator and the condenser, have not yet been considered. Experimental investigations have shown that working-fluid mixtures are likely to experience lower HTCs than pure fluids under similar conditions. Thus, it is imperative to examine the consequences of selecting fluid mixtures on the heat transfer processes in an ORC system, with a view towards determining the sizes and costs of the main system components, and therefore their contributions to overall system cost. The pump and expander costs depend on their power ratings and volume/pressure ratios, which were derived from the thermodynamic optimization and thus need no further treatment. The costs of the heat exchangers on the other hand depend on their sizes, which cannot be obtained from thermodynamic calculations alone, and require appropriate heat transfer models.

### 3.1 Heat Exchanger Sizing

The heat addition process is carried out in two heat exchangers: (1) the Preheater (Ph), used to pre-heat the working fluid to saturated liquid; and (2) the Evaporator (Ev), used to evaporate the working fluid to the saturated vapour state. Similarly, the heat rejection process is carried out in the Desuperheater (Dsh) and the Condenser (Cn). All heat exchangers are modelled as counter-current, shell-and-tube exchangers (shell and tube diameters: 70 mm and 25 mm; tube thickness: d$x$ = 5 mm) constructed from carbon-steel (thermal conductivity: $k$ = 51 W.m$^{-1}$.K$^{-1}$), and are discretized into 100 (variable-sized) segments, $i$ (= 1 – 100), each segment having an equal heat transfer/duty, *i.e.*, $\dot{Q}_{\text{in}}/100$ or $\dot{Q}_{\text{out}}/100$. In all heat exchangers, the working fluid flows through the tube-side (tb), while the heat source and sink streams are the shell-side (sh) fluids. Thus, the total rates at which heat is transferred to/from the working fluid in relation to Equations (2) and (4), respectively, are given by:

$$\dot{Q}_{\text{in}} = \dot{Q}_{\text{Ph}} + \dot{Q}_{\text{Ev}} = \sum_{i=1}^{100} \dot{Q}_i + \sum_{i=1}^{100} \dot{Q}_i \text{ ; and, } \dot{Q}_{\text{out}} = \dot{Q}_{\text{Dsh}} + \dot{Q}_{\text{Cn}} = \sum_{i=1}^{100} \dot{Q}_i + \sum_{i=1}^{100} \dot{Q}_i \,. \tag{5}$$

Furthermore, for each segment an overall heat-transfer coefficient, $U_i$, can be defined such that:

$$\dot{Q}_i = U_i \, A_i \, \Delta T_{\text{lm},i} \text{ ; where:} \tag{6}$$

$$\Delta T_{\text{lm},i} = \frac{(T_{\text{sh},i+1} - T_{\text{tb},i}) - (T_{\text{sh},i} - T_{\text{tb},i-1})}{\ln[(T_{\text{sh},i+1} - T_{\text{tb},i})/(T_{\text{sh},i} - T_{\text{tb},i-1})]} \text{ ; and, } U_i^{-1} = h_{\text{sh},i}^{-1} + dx/k + h_{\text{tb},i}^{-1} \,. \tag{7}$$

Single-phase local HTCs ($h_{\text{sh}}$, $h_{\text{tb}}$) can be calculated by using the Dittus-Boelter Nusselt number ($\text{Nu}_{i,\text{sp}}$) correlation, whereas two-phase HTCs can be calculated by suitably modifying $\text{Nu}_{i,\text{sp}}$ with empirical functions of the Martinelli parameter, $X_{\text{tt}}$ (Jung et al., 1989; Shin et al., 1996). In the present work, this modification was fitted specifically to results from experiments involving horizontal turbulent-flow boiling of refrigerant mixtures, as:

$$\text{Nu}_{i,\text{tp}} = \text{F}(X_{\text{tt}}) \, \text{Nu}_{i,\text{sp}} \text{ ; where: } \text{F}(X_{\text{tt}}) = 1 + 1.8 X_{\text{tt}}^{-0.82} \text{ , and } X_{\text{tt}} = \left(\frac{1-q}{q}\right)^{0.9} \left(\frac{\rho_{\text{v}}}{\rho_{\text{l}}}\right)^{0.5} \left(\frac{\mu_{\text{l}}}{\mu_{\text{v}}}\right)^{0.1} \,. \tag{8}$$

Equation (8) can be applied directly for pure fluids using the overall mixture composition for the liquid and vapour-phase properties. For the fluid mixtures, $X_{tt}$ is calculated using the equilibrium liquid and vapour-phase compositions (not the overall composition) at the saturation temperature and corresponding vapour quality, $q$ on mass basis (Jung et al., 1989). The HTAs of all segments are then calculated from Equation (6) and summed to give the total HTA ($A_{HX}$) for the heat exchanger of interest.

### 3.2 Heat Exchanger Sizing for Optimal Cycles

First, we verify the overall HTCs calculated using Equations (7) – (8), especially for the heat exchangers involving phase change (Evaporator and Condenser). The overall HTCs at the 20$^{th}$, 50$^{th}$ and 80$^{th}$ segments of these heat exchangers, and for the single-phase heat exchangers, are presented in Figure 3 for the R-245fa + R-227ea system. The calculated values are in good general alignment with the experimental data obtainable for flow boiling of refrigerant mixtures found in Jung et al. (1989) and Shin et al. (1996). Also in agreement with experimental observations, the HTCs for the working-fluid mixtures at each of the segments appear lower than the linearly interpolated values between the two pure-fluid components that make up the mixture. While various explanations have been proposed for this phenomenon, most authors contend that it is due to mass-transfer effects caused by the composition differences between the vapour and liquid phases during the phase-change process.

In the single-phase heat exchangers (Preheater and Desuperheater), the overall HTCs for the mixtures are also lower than the linearly interpolated values, although this deviation is less pronounced for the R-245fa + R-227ea mixtures. Overall, the HTCs are highest in the Evaporator, followed by the Condenser, and lowest in the Desuperheater. Higher HTCs are achieved in the Condenser and Evaporator due to change of phase. The working-fluid vapour results in the low HTC values in the Desuperheater.

Based on the knowledge of the HTCs and the associated heat-transfer rates, the HTAs for all segments of the heat exchangers can be calculated from Equation (6). The HTAs of the segments in the Evaporator and the Condenser (for R-245fa + R-227ea) are presented in Figure 4; similar observations can be made by considering *n*-pentane + *n*-hexane. As the mole fraction of R-227ea is increased in the mixture, the HTA is seen to increase and then decrease such that the pure fluids (R-245fa and R-227ea) have heat exchangers with the lowest HTAs. This is the case across all of the segments and in both the Evaporator and the Condenser as a direct result of the lower HTCs of the working-fluid mixtures, with the only exception being that of the Evaporator for R-245fa + R-227ea where some mixtures (*e.g.*, $x_{R\text{-}227ea} = 0.8$) have lower HTAs than pure R-245fa; pure R-227ea still has the lowest areas across all of the sections.

The HTA variations are less pronounced in the Evaporator than in the Condenser where large differences exist between the pure fluids and the mixtures. The pure fluids have the smallest areas primarily due to their higher HTC values. For example, even though the Evaporator for the case of pure *n*-hexane has the highest heat-transfer rate (see Table 1), it has the smallest areas because *n*-hexane has the highest overall HTC amongst all the working fluids. In a similar manner, although the condenser for pure R-245fa has the highest duty, its high HTC enables it to have a lower HTA than those of the mixtures.

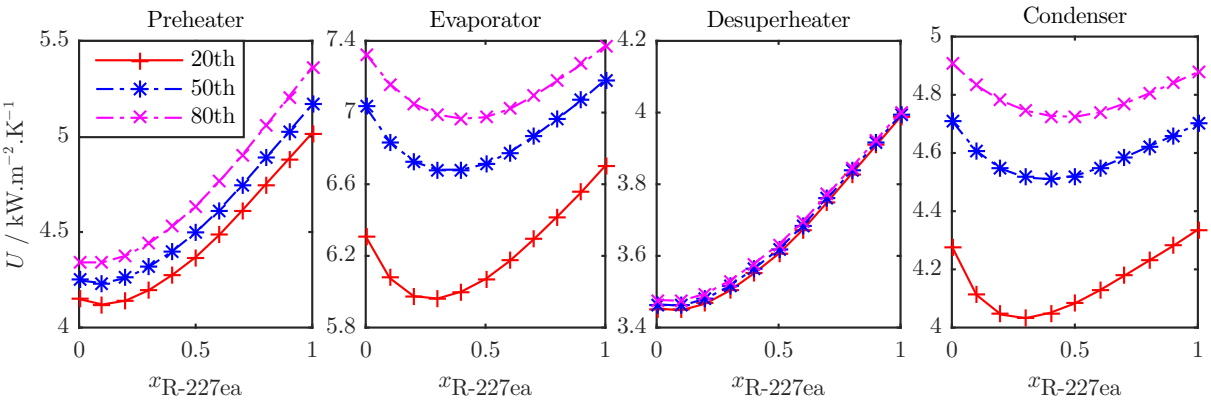


**Figure 3: Overall HTCs at segments along the heat exchangers for R-245fa + R-227ea system**

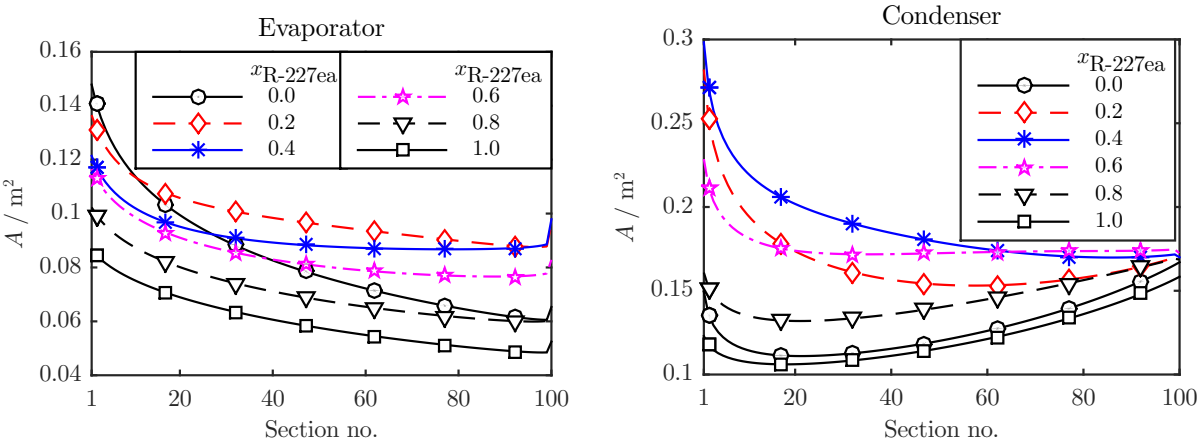


**Figure 4: Heat-transfer areas along the Evaporator and Condenser for R-245fa + R-227ea system**

The total HTAs for each of the heat exchangers with the different working-fluid mixtures are presented in Figure 5. As expected by consideration of their thermal duties (see Table 1), the Evaporators are generally three times as large as the Preheaters, while the Condensers are 8 – 13 times larger than the Desuperheaters. Although the Condenser thermal-duties are only about 15% higher than those of the Evaporators, the Condensers are twice as large as the Evaporators in most instances. This is due to the lower overall HTCs and the lower temperature differences across the Condensers.

As the concentration of R-227ea in the refrigerant-mixture system is increased, the Ph and Dsh heat duties increase, and so do the total HTAs of both heat exchangers. The Dsh area reaches a maximum at 90 mol% R-227ea and then decreases slightly for pure R-227ea. The Dsh and Ph areas for the *n*-pentane + *n*-hexane systems are also directly governed by their heat duties. It should however be noted that these variations in HTA with working-fluid mixtures (range of 0.13 m$^2$ and 0.10 m$^2$; 1.12 m$^2$ and 0.31 m$^2$) are much smaller than those associated with the two-phase heat exchangers. This is important, in that it suggests that working-fluid mixtures have a more profound effect on the Evaporator and Condenser sizes than they do on the single-phase heat-exchangers, at least in the present study.

From Figure 5, it is clear that the pure working-fluids have smaller Evaporator HTAs compared to the mixtures. The only exception is found in the R-245fa + R-227ea system, where fluid mixtures with $x_{R\text{-}227ea} \geq 0.6$ have lower Ev areas than pure R-245fa. Furthermore, due to the deterioration of HTCs during condensation, the Condensers for the working-fluid mixtures are much larger than those for the pure fluids. In the case of the R-245fa + R-227ea system, the HTAs range from 12.2 m$^2$ ($x_{R\text{-}227ea} = 1$) to 18.8 m$^2$ ($x_{R\text{-}227ea} = 0.4$), representing a difference of 54%. Such large differences in HTAs between working-fluid mixtures and pure fluids can lead to considerable differences in plant size and cost.

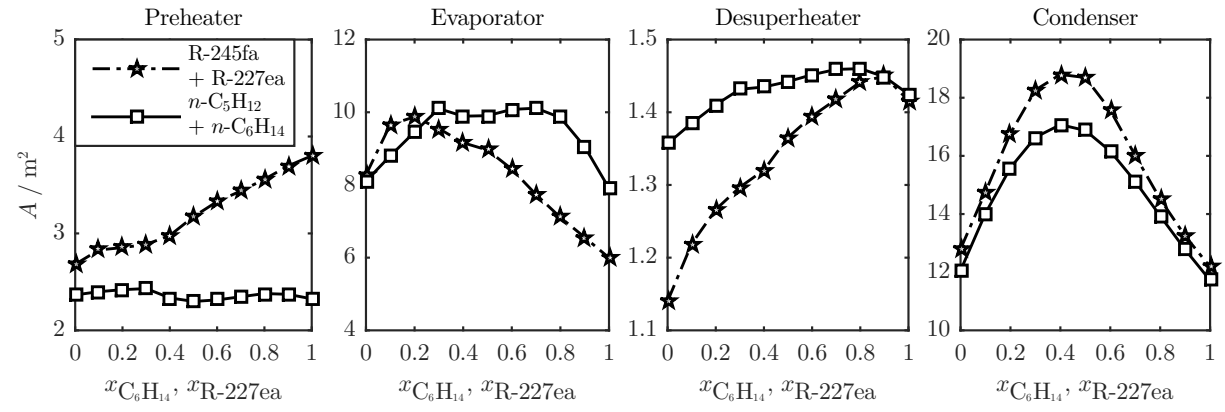


**Figure 5: Total heat-transfer areas for heat exchangers with the different working-fluid mixtures**

## 4. COST ANALYSIS OF OPTIMAL CYCLES

We conclude this paper with a brief investigation of the cost implications of employing working-fluid mixtures in ORC systems. The key components affected by the choice of working fluid are those illustrated previously – the working-fluid pump, the expander and the heat exchangers. The costs of these components are added to give an estimate of the plant cost. Although this sum does not give the total installation cost, it is through this amount that the effects of working-fluid choice on plant costs are manifested directly. Other factors that contribute to the plant installation costs would be similar for the various working fluids considered. Component-base costs ($C_B$, indexed in year 2006; £1 ≡ €1.47, $1.84) are calculated using logarithmic correlations of component size factors ($S$) according to Seider et al. (2009) and are presented in Table 2. Also in Table 2 are the cost coefficients (converted to SI units). The calculated component-base costs of the optimal cycles are presented in Figure 6 (LHS axes).

**Table 2: Component cost coefficients used in $C_B = (F)\exp\{C_0 + C_1[\ln S] + C_2[\ln S]^2\}$**

| Component | $S$ | F | $C_0$ | $C_1$ | $C_2$ |
|---|---|---|---|---|---|
| Pump | $\dot{V}\sqrt{H}$ ($m^3.s^{-1}.m^{1/2}$) | 2.7 | 9.0073 | 0.4636 | 0.0519 |
| Expander | $\dot{W}_{exp}$ (kW) | 1.0 | 6.5106 | 0.8100 | 0.0000 |
| Expander* | $\dot{W}_{exp}$ (kW) | 1.0 | 7.3194 | 0.8100 | 0.0000 |
| Heaters/Coolers | $A$ ($m^2$) | 1.0 | 10.1060 | -0.4429 | 0.0901 |
| Evaporator/Condenser | $A$ ($m^2$) | 1.0 | 9.5638 | 0.5320 | -0.0002 |

* Sub-atmospheric pressure discharge expander (applicable to $x_{C_6H_{14}} \geq 0.1$)

The pumps cost around £5,200, with the cost reducing monotonically from pure *n*-pentane (R-227ea) to *n*-hexane (R-245fa) as a direct result of the lower evaporation pressures as the concentration of *n*-hexane (R-245fa) in the working fluid is increased (in line with Figure 1). Similarly, the costs of the single-phase heat exchangers (Ph and Dsh) are low (£5,000 – £6,000). However, the evaporator and condenser costs are well in excess of £25,000. The expander costs fall into two classes: (i) sub-atmospheric pressure discharge expanders that cost about £35,000; and (ii) standard expanders with a considerably lower cost of about £15,000. From these results, it is clear that the expander and the phase-change heat exchangers present the dominant costs of the ORC system considered here.

The pure fluids (pure *n*-pentane and *n*-hexane; R-245fa and R-227ea) generally have the lowest-cost evaporators and condensers, while the mixtures ($x_{C_6H_{14}} = 0.7$ and $x_{C_6H_{14}} = 0.4$; $x_{R\text{-}227ea} = 0.2$ and $x_{R\text{-}227ea} = 0.4$ respectively) have the highest costs. The condenser size and cost is smallest for *n*-pentane despite it having a larger heat duty and working-fluid flow-rate (see Table 1) than those for the mixtures.

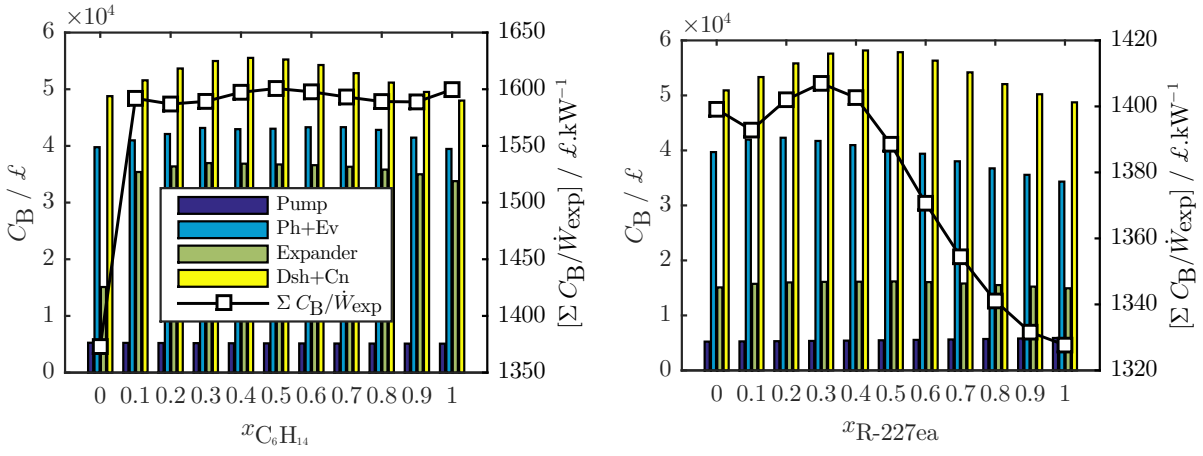


(a) *n*-pentane + *n*-hexane (b) R-245fa + R-227ea

**Figure 6: Optimal cycles' component costs (bars; LHS axes) and cost per kW (line; RHS axes)**

From Figure 6a and 6b, it is clear that the expander costs mirror the trend exhibited by the optimal power output in Figure 1a and 1b especially as they are correlated with the power output. However, for the *n*-pentane + *n*-hexane system, the expander cost for pure *n*-pentane ($x_{C_6H_{14}} = 0$) is over 50% lower than those of the other working fluids. After expansion, the *n*-pentane vapour exits the expander at above atmospheric pressure while all the other fluids exit at sub-atmospheric pressures and had their expander costs calculated with the low-pressure discharge expander correlation in Table 2. This in turn makes the cost of the *n*-pentane expander much lower than the rest.

We complete the analysis by considering the 'rated costs' for the optimal cycles, *i.e.*, cost per kilowatt of power generated ($\Sigma C_B/\dot{W}_{exp}$). This is done such that high power output fluids (especially the fluid mixtures) are not unnecessarily penalized. The rated costs of the optimal cycles are plotted in Figures 6a and 6b (RHS axes). As expected, the ORC system with *n*-pentane as the working fluid has the lowest rated cost (£1,370/kW) due to its very low expander cost compared to the other working fluids while the cycle with $x_{C_6H_{14}} = 0.5$ has the highest rated cost at £1,600/kW. For the R-245fa + R-227ea system, the ORC system with pure R-227ea has the lowest rated cost (£1,330/kW) while that with $x_{R\text{-}227ea} = 0.3$ has the highest rated cost. The previously identified, thermodynamically optimal fluid mixtures ($x_{C_6H_{14}} = 0.3$ and $x_{R\text{-}227ea} = 0.5$; see Figure 1) have cycle rated costs of £1,600/kW and £1,400/kW respectively. On the other hand, the cost optimal working fluids are *n*-pentane and R-227ea, which give rated cost reductions of 14% and 5% respectively over the thermodynamically optimal working fluids.

## 5. CONCLUSIONS

The first aim of this study was to investigate the thermodynamic benefits of employing working-fluid mixtures in organic Rankine cycle (ORC) systems, and a second aim was to examine the effects of selecting such mixtures on the sizes and costs of the resulting ORC engines. Two sets of fluid mixtures, namely *n*-pentane + *n*-hexane and R-245fa + R-227ea, were used for this investigation due to their common use in ORC installations. A low-temperature geothermal hot-water heat-source stream was considered. The thermodynamic optimization (maximum expansion power output) resulted in optimal working-fluid mixtures in both cases; the performance indices of these mixtures along with corresponding costs are summarized and compared with those of their constituent pure components in Table 3 below.

**Table 3: Performance indices and costs of pure fluids and thermodynamically optimal mixtures**

| $x_{C_6H_{14}}$ | $\dot{W}_{exp}$ kW | *PR* - | *VR* - | $A_{Ev}$ m$^2$ | $A_{Cn}$ m$^2$ | $\Sigma C_B/\dot{W}_{exp}$ £/kW | $x_{227ea}$ | $\dot{W}_{exp}$ kW | PR - | VR - | $A_{Ev}$ m$^2$ | $A_{Cn}$ m$^2$ | $\Sigma C_B/\dot{W}_{exp}$ £/kW |
|---|---|---|---|---|---|---|---|---|---|---|---|---|---|
| 0.0 | 79.3 | 3.42 | 3.45 | 8.11 | 12.1 | 1370 | 0.0 | 79.3 | 3.38 | 3.55 | 8.28 | 12.8 | 1400 |
| 0.3 | 88.3 | 4.51 | 4.50 | 10.1 | 16.6 | 1590 | 0.5 | 86.4 | 3.73 | 4.30 | 8.96 | 18.7 | 1390 |
| 1.0 | 79.0 | 4.15 | 4.09 | 7.91 | 11.7 | 1600 | 1.0 | 78.3 | 2.88 | 3.75 | 6.00 | 12.2 | 1330 |

The analyses revealed that the temperature glides of the working-fluid mixtures during evaporation and condensation resulted in higher power output and thermal/exergy efficiencies for fluid mixtures. Mixtures containing 30 mol% of *n*-hexane 50 mol% R-227ea had the highest output, more than either set of pure fluids. The pure fluids did however result in smaller expanders due to their low volumetric flow-rates and expansion ratios. Fluid mixtures appeared to have the largest evaporators and condensers, requiring more expensive heat exchangers than the pure fluids. Moreover, due to sub-atmospheric expansion, the expander costs in the case of the *n*-pentane + *n*-hexane working-fluid mixtures (and *n*-hexane) were much higher than those for pure *n*-pentane. Generally, equipment sizes and costs were larger for both set of mixtures than for the constituent pure fluids. Thus, the working-fluid mixtures would require larger plant layout areas, contributing significantly to their overall installation costs.

Although the mixtures were found to have the highest power output, they also had the highest rated cost (equipment cost per kilowatt power generated). On the other hand, ORC systems with pure *n*-pentane working had the lowest rated cost followed by those with *n*-hexane. For the case of R-245fa + R-227ea

working fluids, pure R-227ea had the lowest rated costs. These observations imply that the thermodynamic benefits derived from using the working-fluid mixtures may be outweighed by the increased costs incurred. The fact that these insights were only possible from a direct consideration of thermal and cost factors as exemplified here, underlines the importance of employing a combined thermodynamic, thermal and cost approach in the selection of optimal working-fluid (mixtures) for ORC systems.

## REFERENCES


Aghahosseini, S. and Dincer, I. (2013). Comparative performance analysis of low-temperature organic Rankine cycle (ORC) using pure and zeotropic working fluids. *Applied Thermal Engineering*, 54(1):35–42.

Angelino, G. and di Paliano, P. C. (1998). Multicomponent working fluids for ORCs. *Energy*, 23(6):449–463.

Beardsmore, G., Budd, A., Huddlestone-Holmes, C., and Davidson, C. (2015). Country update—Australia. In *Proceedings World Geothermal Congress 2015*, pages 19–24.

Braimakis, K., Leontaritis, A.-D., Preißinger, M., Karellas, S., Brüggeman, D., and Panopoulos, K. (2014). Waste heat recovery with innovative low-temperature ORC based on natural refrigerants. In *27st International Conference on Efficiency, Cost, Optimization, Simulation and Environmental Impact of Energy Systems*.

Byrd, R., Hribar, M., and Nocedal, J. (1999). An interior point algorithm for large-scale nonlinear programming. *SIAM Journal on Optimization*, 9(4):877–900. doi: 10.1137/S1052623497325107; 26.

Chen, H., Goswami, D. Y., Rahman, M. M., and Stefanakos, E. K. (2011). A supercritical Rankine cycle using zeotropic mixture working fluids for the conversion of low-grade heat into power. *Energy*, 36(1):549–555.

Chys, M., van den Broek, M., Vanslambrouck, B., and Paepe, M. D. (2012). Potential of zeotropic mixtures as working fluids in organic Rankine cycles. *Energy*, 44(1):623–632.

Dong, B., Xu, G., Cai, Y., and Li, H. (2014). Analysis of zeotropic mixtures used in high-temperature organic Rankine cycle. *Energy Conversion and Management*, 84(0):253–260.

Garg, P., Kumar, P., Srinivasan, K., and Dutta, P. (2013). Evaluation of isopentane, R-245fa and their mixtures as working fluids for organic Rankine cycles. *Applied Thermal Engineering*, 51(1–2):292–300.

Heberle, F., Preißinger, M., and Brüggemann, D. (2012). Zeotropic mixtures as working fluids in organic Rankine cycles for low-enthalpy geothermal resources. *Renewable Energy*, 37(1):364–370.

Jung, D. S., McLinden, M., Radermacher, R., and Didion, D. (1989). Horizontal flow boiling heat transfer experiments with a mixture of R22/R114. *International Journal of Heat and Mass Transfer*, 32(1):131–145.

Kunz, O. and Wagner, W. (2012). The GERG-2008 wide-range equation of state for natural gases and other mixtures: An expansion of GERG-2004. *Journal of Chemical & Engineering Data*, 57(11):3032–3091.

Lampe, M., Kirmse, C., Sauer, E., Stavrou, M., Gross, J., and Bardow, A. (2014). Computer-aided molecular design of ORC working fluids using PC-SAFT. *Computer Aided Chemical Engineering*, 34(0):357–362.

Lecompte, S., Ameel, B., Ziviani, D., van den Broek, M., and Paepe, M. D. (2014). Exergy analysis of zeotropic mixtures as working fluids in organic Rankine cycles. *Energy Conversion and Management*, 85:727–739.

Lemmon, E. W., Huber, M. L., and McLinden, M. O. (2013). NIST standard reference database 23: Reference fluid thermodynamic and transport properties-REFPROP.

Li, Y.-R., Du, M.-T., Wu, C.-M., Wu, S.-Y., and Liu, C. (2014). Potential of organic Rankine cycle using zeotropic mixtures as working fluids for waste heat recovery. *Energy*, 77(0):509–519.

Oyewunmi, O. A., Taleb, A. I., Haslam, A. J., and Markides, C. N. (2014). An assessment of working-fluid mixtures using SAFT-VR Mie for use in organic Rankine cycle systems for waste-heat recovery. *Computational Thermal Sciences: An International Journal*, 6(4):301–316.

Papadopoulos, A. I., Stijepovic, M., and Linke, P. (2010). On the systematic design and selection of optimal working fluids for organic Rankine cycles. *Applied Thermal Engineering*, 30(6–7):760–769.

Sami, S. M. (2010). Energy and exergy analysis of new refrigerant mixtures in an organic Rankine cycle for low temperature power generation. *International Journal of Ambient Energy*, 31(1):23–32.

Seider, W. D., Seader, J. D., and Lewin, D. R. (2009). *Product & Process Design Principles: Synthesis, Analysis And Evaluation*. John Wiley & Sons.

Shin, J. Y., Kim, M. S., and Ro, S. T. (1996). Correlation of evaporative heat transfer coefficients for refrigerant mixtures. In *International Refrigeration and Air Conditioning Conference*, page 316.

Shu, G., Gao, Y., Tian, H., Wei, H., and Liang, X. (2014). Study of mixtures based on hydrocarbons used in ORC (organic Rankine cycle) for engine waste heat recovery. *Energy*, 74(0):428–438.

Wang, J. L., Zhao, L., and Wang, X. D. (2010). A comparative study of pure and zeotropic mixtures in low-temperature solar Rankine cycle. *Applied Energy*, 87(11):3366–3373.